Environmental Nanotechnology, Monitoring & Management 16 (2021) 100541

Contents lists available at ScienceDirect

Environmental Nanotechnology, Monitoring & Management

journal homepage: www.elsevier.com/locate/enmm

Synthesis, performance and mechanism of nanoporous Fe-(1,3,5-tricarboxylic acid) metal-organic framework in the removal of anionic dyes from water

José Elías Conde-González [a], Eladia M. Peña-Méndez [a,*], Alba M. Melián-Fernández [a], Josef Havel [b], Victoria Salvadó [c]

[a] Departamento de Química, Unidad Departamental de Química Analítica, Facultad de Ciencias, Universidad de La Laguna, Avda. Astrofísico Fco. Sánchez, s/n, 38206 La Laguna, Spain
[b] Department of Chemistry, Faculty of Science, Masaryk University, Kamenice 5/A14, 625 00 Brno, Czech Republic
[c] Department de Química, Facultat de Ciències, Universitat de Girona, C/ Mª Aurèlia Capmany, 69, 17003 Girona, Spain

ARTICLE INFO

Keywords:
Nano Fe-BTC
MOFs
Water quality
Anionic dyes
Adsorption
D-SPE

ABSTRACT

The direct synthesis of nano-{Fe-BTC} MOFs was performed following green chemistry rules. This nanomaterial has been characterized by several techniques showing structural similarities with commercial Fe-BTC MOFs, although it has greater porosity due to the presence of mesopores and micropores, that can make it an efficient adsorbent for fluorescent anionic dyes through electrostatic and π-π interactions between dye and nano-{Fe-BTC}. The adsorption isotherms fit the Freundlich model: tetrabromo-fluorescein(Br-FL) has the highest K_F value, followed by dichloro-fluorescein(Cl-FL) and fluorescein(FL). The kinetic study suggests that the adsorption onto nano-{Fe-BTC} follows the pseudo-second-order model and the adsorption capacities follow the order Br-FL (q_e 0.836 mg·g^{-1}) > FL (q_e 0.106 mg·g^{-1}) ~Cl-FL (q_e 0.100 mg·g^{-1}), pH = 4. The use of methanol (5% NH_3) allows recoveries of the dyes from nano-{Fe-BTC} ranging from 90% to100%. The presence of inorganic ions and organic substances in the water solution does not affect the adsorption of the dyes even when possible interfering species were present at concentrations that were up to 10^9 times higher than that of the dyes. The method was successfully applied to remove the target dyes from spiked water samples, showing the potential of high porous nano-{Fe-BTC} MOFs as a promising adsorbent for the effective removal of dyes from waters.

1. Introduction

Dyes, classified by both the US EPA and the European Union as hazardous residues, and other colourants from different industrial and domestic sources are a major source of water contamination. Their elimination has not been sufficiently addressed and inadequately treated wastewater can affect the quality of water bodies (streams, lakes and aquifers) as well as drinking water and limiting the access to it (Directive 2008/98/EC; Commission notice 2018/C 124/01; EPA 820-R-11-003; EPA530-F-05-004). The pollutants are not only the compounds that make up the dyes but also their decomposed products, such as radicals, and toxic organic compounds (UN World Water Development Report, 2015; McAvoy, 2014; Pereira and Alves, 2012). All of them represent a significant danger both to human health and aquatic life, especially in fish, and affecting light penetration and temperature of water bodies (Hossain et al., 2016; Preiß et al., 2017). Existing treatments of wastewater to remove dyes are costly and time-consuming and are mostly not sufficiently effective for the established water quality standards to be reached (Directive 2008/98/EC; Commission notice 2018/C 124/01; EPA 820-R-11-003; EPA530-F-05-004; UN World Water Development Report, 2015). Therefore, there is a clear need to explore and develop new and improved technologies.

Organic dyes contain chromophore or auxochrome groups (–OH, –NH_2, –OR, –NHR, and –NR_2) in their structure, which define the ability of these compounds to absorb visible light. Xanthene anionic dyes, particularly those containing chlorine and bromine in their structure, such as dichlorofluorescein and tetrabromofluorescein (Fig. 1), are regarded as being especially toxic (Hossain et al., 2016; Alvarez et al., 2017; Preiß et al., 2017; Lilly et al., 2018; Oliveira et al., 2018; Ortiz-Perea et al., 2018). Fluorescein (FL), dichlorofluorescein (Cl-FL) and

* Corresponding author.
E-mail address: empena@ull.edu.es (E.M. Peña-Méndez).

https://doi.org/10.1016/j.enmm.2021.100541
Received 24 September 2020; Received in revised form 8 July 2021; Accepted 4 August 2021
Available online 8 August 2021

tetrabromofluorescein (Br-FL) are selected in this study as representative of anionic dyes, which are aromatic pollutants found in water that are mainly of industrial origin; amongst other uses they are found in textiles, paper, printing, and photographic materials. Moreover, Cl-FL is used as a probe for following intracellular mechanisms of solar water disinfection, FL and Br-FL have been identified as photosensitizers of cell-compatible polymer coatings, and fluorescein has been used as a drug model (Alan and Tang, 2014; Castro-Alférez et al., 2016; Mohamed and El Nemr, 2017; Ponnusamy and Saravanan, 2017; Lilly et al., 2018; Chatha et al., 2019).

Different review articles cover the variety of materials used to extract dyes from water bodies (Xiaokun and Bo, 2016; Aderonke et al., 2012; Chatha et al., 2019). Among these, metal organic frameworks (MOFs) are interesting compounds with an increasing number of applications, including the removal of contaminants, catalysis, gas storage, drug carriers, and biomedicine (Aderonke et al., 2012; Tao et al., 2016; Diercks et al., 2018). MOFs have properties that cannot be attained in either molecular coordination complexes or other classes of extended structures. One of the most important properties of MOFs is flexibility, which is missing in materials such as zeolites (Bennett et al., 2010; Horcajada et al., 2010; Bennett and Cheetham, 2014; Sánchez-Sánchez et al., 2015; Cheetham et al., 2016; Lee et al., 2019). In studies by Cheetham et al. (2016) and Bennett et al. (2010), Bennett and Cheetham (2014) it was found that flexibility, defects, and disorder in the structure of MOFs are not just prevalent in MOF disorder and that their applications are different, as can be seen, for example, with the adsorption of volatile and other compounds. The synthesis of MOFs has undergone an evolution, from complex procedures such as solvo-thermal and non solvo-thermal, electrochemical, microwave, mechano-chemical, sonochemical synthesis (Aderonke et al., 2012; Tao et al., 2016; Diercks

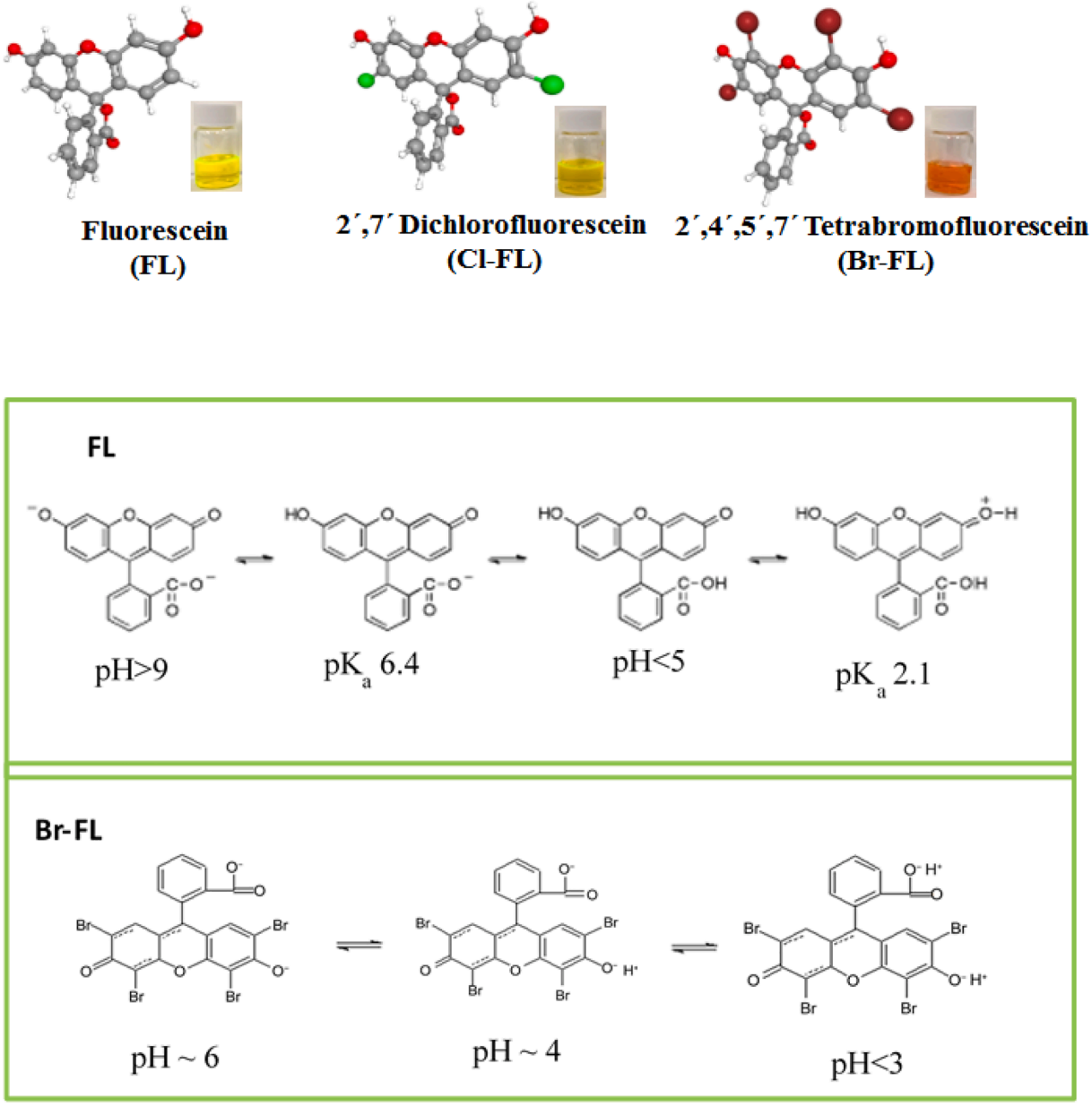

Fig. 1. Chemical structure of Dyes. Ionization chemical equilibria for FL and Br-FL. Adapted from Hossain et al. and Oliveira et al. (Cheetham et al., 2016, Directive 2008/98/EC).

et al., 2018; Chatha et al., 2019), which are often difficult to reproduce and unscalable, to newer methods that are more simple, reproducible and scalable (Bennett et al., 2010; Cheetham et al., 2014; Horcajada et al., 2010).

Recently, Fe-BTC MOFs, an Fe-based MOF material, which has Fe(III) as the metal centre and trimesic acid (1,3,5-benzenetricarboxylate; BTC) as an organic linker, was identified as a valuable and promising material for selective adsorption processes, drug transport, catalysis, and sensing. Particular emphasis is placed on Fe-BTC MOFs' diverse structure, easy functional surface tunability, high porosity, and high surface area, among other properties. Moreover, this Fe-BTC MOFs is biocompatible and environmentally friendly and can be synthesized by different routes. The differences between various forms of Fe-BTC (Material of Institute of Lavoisier MIL 100 (Fe) and commercial Basolite®F300) are presented in Table 1. The rapid development without precedent of these nanoporous Fe-BTC MOFs materials led to various potential applications for host compounds with different physico-chemical properties, platforms for testing different drugs in medicine (Amarajothi et al., 2012; Preiß et al., 2017; Lee et al., 2019; Peña-Méndez et al., 2020), adsorption of organic and inorganic compounds (Diercks et al., 2018; Saravanan and Anbalagan, 2017), amongst others. The complication and expense involved in the synthesis of MOF compounds make it difficult to scale up as it is time-consuming and uses toxic organic solvents. Recently, new alternative routes to directly synthesise nano-{Fe-BTC} MOFs have been explored without loss of the advantages of the physical and chemical properties (Horcajada et al., 2010; Lee et al., 2019; Peña-Méndez et al., 2020).

The present study has two main objectives: i) to investigate a direct environmentally sustainable route of synthesis to produce nano-{Fe-BTC} MOFs with high surface area and porosity, ii) to evaluate the adsorption of various anionic dyes (fluorescein, dichlorofluorescein and tretrabromofluorescein) from water, providing support as a model for the removal of small molecules from polluted waters.

2. Experimental and material section

2.1. Materials

Fluorescein sodium salt (FL, CAS 518-47-8), 2′,7′-Dichlorofluorescein sodium salt (Cl-FL, CAS 80471-69-8), 2′,4′,5′,7′-Tetrabromofluorescein Sodium Salt (Br-FL, Eosyn Y, CAS 15086-94-9), Iron (III) chloride hexahydrate and hydrochloric acid were purchased from Fluka Chemie AG, (Buchs, Switzerland). Ethanol (EtOH), methanol (MeOH), acetonitrile (AcN), trimesic acid (benzene-1,3,5-tricarboxylic acid, H_3BTC), 4-[3-(4-Carboxylatophenyl)-5-[4-(dihydroxymethyl) phenyl]phenyl]benzoate (PTA), Basolite®F300, Basolite® C300, Basolite® Z377, and sodium hydroxide were purchased from Sigma-Aldrich Chemie GmbH (Steinheim, Germany). Deionised water was obtained using a Milli-Q gradient system A10 from Millipore (Bedford, MA, USA). All glassware was rinsed with 10% nitric acid and Milli-Q water several times before use. Iso-disc™ filters, PTFE-4-2, 4 mm × 0.2 μm from Supelco (Bettelfonte, PA, USA). Working solutions were prepared by appropriate dilution of the stock solution with ultrapure water. All chemicals were of analytical reagent grade unless otherwise indicated and were used as received without further purification.

Table 1
Comparison of published data for MIL-100(Fe), Basolite®F300, and Fe-BTC MOF Basolite like materials*.

Material*	S_{BET} ($m^2 \cdot g^{-1}$)	V_{pore} ($m^3 \cdot g^{-1}$)	Pore (Å)	Reference
Basolite®F300	1300–1600	–	25–29	Sigma-Aldrich
Basolite*	840	0.38	21.7	Horcajada et al. (2010); Amarajothi et al. (2012)
Fe-BTC Basolite like	1125	0.61	–	Bennett et al. (2010)
Fe-BTC Basolite like	1010	0.9	–	Horcajada et al. (2010)

*name for description of the materials given by authors. – not published data.

2.2. Synthesis of the Nano-{Fe-BTC} MOFs

The synthesis of Nano-{Fe-BTC} MOF material (BTC: 1,3,5-benzenetricarboxylate) was carried out via the reaction of BTC in basic media with ferric chloride hexahydrate ($FeCl_3 \cdot 6H_2O$) in water at room temperature: 2.63 g BTC and 1.5 g NaOH were dissolved in 100 mL Milli-Q water. A 100 mL solution containing 5.08 g $FeCl_3$ was added to the previous one, dropwise, at a constant rate of 1 mL/min using a peristaltic pump with continuous mechanical stirring (T = 25 °C), leading to the immediate formation of light orange solids. After the addition was finished, the resultant suspension was mechanically stirred for 1 h to ensure complete reaction. Afterwards, the suspension was centrifuged; the product was washed with deionised water and ethanol, and finally dried at 120 °C for 24 h. The homogenisation of the material was done by ZrO ball milling using a Spex 8000 apparatus. After 60 min milling time, the powder was washed with ethanol and dried in air at 100 °C.

2.3. Apparatus and instrumentation

A pH meter (PH 197-S) equipped with a SenTix-81 pH electrode from WTW (Weilheim, Germany), an Inlab® micro-pH electrode from Mettler Toledo (Barcelona, Spain), a peristaltic pump model 203 from Scientific Industries, Inc. (Bohemia, New York, USA), a magnetic stirrer hotplate from IKA®-Werke GmbH & Co. KG (Staufen, Germany), a mechanical shaker (Selecta Rotabit).

HPLC analysis was performed using a Varian ProStar-LC HPLC system equipped with a quaternary pump, auto sampler model 410, and fluorescence detector using Galaxie Workstation Chromatography Data System software (Varian Inc., Australia). The separation was carried out at 303 K using a Microsorb-MV 100–8 C18 HPLC column (250 mm × 4.6 mm × 1/4″) and a Chromguard HPLC SS 10 mm × 3 mm pre-column, which were both from Varian Inc. (California, USA). Fluorescence detector conditions were Br-FL (λexc = 520 nm, λemi = 570 nm), FL (λexc = 438 nm, λemi = 513 nm), and Cl-Fl (λexc = 450 nm, λemi = 524 nm). The mobile phase was an Andersen buffer (pH 4.46) (A): AcN (B) (70:30, *v/v*) in gradient mode. The flow rate was 1 mL/min and the injection volume was 10 μL. The performance of the analytical method was established by determining the analytical quality parameters (Table 3S).

Different techniques were used to analyse the structure, composition, size, and morphology of the synthesised composite. The particle size distribution and zeta-potential were measured at different pH values using a Malvern Zetasizer Nano ZS, Micromeritics AUTOCHEM 2920, a pH meter equipped with an Inlab® micro-pH electrode from Mettler Toledo (Barcelona, Spain), and an IKA Labourtechnik RCT B S1 stirrer-hot plate from IKA (Staufen, Germany). The specific surface area, pore size distribution, and pore volume were measured by the Brunauer, Emmett and Teller's method (BET) and surface area analyser at 77 K in the range of $0.02 \leq P/P_0 \leq 1.00$ on a Gemini V 2365 Model from Micrometrics (Norcross, GA, USA).

Thermogravimetric analysis (TGA) was carried out using a diamond thermo-gravimetric/differential thermal analyser (Perkin Elmer Instruments, Shelton, USA). The morphology and size of the synthesised materials were examined using transmission electron microscopy (TEM) (JEOL 2010, Tokyo, Japan). A scanning electron microscope (JEOL JSM 6300, Tokyo, Japan) with a resolution of 3.5 nm combined with an Oxford 6699 ATW energy-dispersive X-ray spectrometer was used to determine the surface composition of the materials.

FTIR spectra were recorded on an Agilent Cary 630 FTIR spectrometer (Agilent, Santa Clara, USA) equipped with a diamond attenuated total reflectance (ATR) accessory. Powder X-ray diffraction (XRD) data were collected at 120 K using a Panalytical X'Pert MPD diffractometer.

The instrument was equipped with CuKα radiation and a curved graphite monochromator on the diffracted beam. Data were collected in the 3–70° 2θ range with an 0.02° step width.

2.4. Sample preparation

Tap water was collected from our laboratory; seawater was obtained from the north-east coast of the island of Tenerife; the wastewater sample was obtained from the Valle Guerra wastewater treatment plant (Tenerife, Canary Islands, Spain). The samples were kept in the dark at 4 °C for not more than 48 h before being analysed. The samples were filtered through a 0.45 μm filter (Chromafil® XtraPET-45/25 filter, Macherey-Nagel GmbH & Co, UK) before extraction. Finally, before subjecting the samples to the analysis by high-pressure liquid chromatography (HPLC), they were filtered through 0.20 μm Iso-disc™ filters.

2.5. Evaluation of the adsorption performance of nano-{Fe-BTC} MOFs towards different anionic dyes

To evaluate the dye adsorption on nano-{Fe-BTC} MOFs, the dispersive solid phase extraction (D-SPE) methodology was used. D-SPE methodology: 12 mg of Nano-{Fe-BTC} MOFs were added to a 15 mL vial containing 10 mL of the aqueous standard solution of the sample and vortex dispersed for 20 min. After this, the suspension was centrifuged at 5000 rpm for 5 min. The supernatant aqueous phase was removed with a Pasteur pipette and the solution was analysed by HPLC-FLD. Afterwards, 1 mL of methanol (5% NH_3) × 3 were added to the nano-{Fe-BTC} MOF sorbent in the tube to desorb the dyes while applying vortex dispersion for another 5 min. The supernatant solution (methanol (5% NH_3)) containing the desorbed dyes were filtered (0.20 μm filters) and 10 μL were directly injected and analyzed by HPLC-Fluorescence. The adsorption efficiency in percentage was calculated according to

$$Adsorption\ \ Efficiency(\%) = \frac{C_0 - C_f}{C_0} \bullet 100 \quad (1)$$

where C_0 is the initial feed concentration of dye solution (mg L^{-1}), C_f is the final concentration of dye solution after adsorption (mg L^{-1}) (Peña-Méndez et al., 2020).

3. Result and discussion

3.1. Characterization of nano-{Fe-BTC} MOFs

The nano-{Fe-BTC} MOF material was synthesized via the reaction of H_3BTC in a basic medium with ferric chloride hexahydrate ($FeCl_3 \cdot 6H_2O$) in water at room temperature. This synthetic route allows (i) the synthesis time to be reduced to two hours, shorter than that required for other methods (Xiaoshi et al., 2016), (ii) for a reduction in the number of reagents and the amount that is used (Xiaoshi et al., 2016; Sánchez-Sánchez et al., 2015), and (iii) high yields to be obtained (cf. Supplementary material). The PXRD patterns of the synthesized nanomaterial (Fig. 2) and commercial Basolite®F300 were compared in terms of relative and absolute intensities, and the position of the diffraction bands, showing a very good fit with the material synthesized by Sánchez-Sánchez et al. (2015) and Pilloni et al. (2015). The diffraction peaks of the synthesized nano-{Fe-BTC} MOFs, which are characteristic of the crystalline order and similar to those of commercial Basolite®F300, reveal that the basic building blocks and connectivity of the crystalline counterparts are maintained. The broad peak shapes seen in the diffractogram are most like those due to a small crystallite size (Oliveira et al., 2018).

The infrared spectra of the commercial Basolite®F300 and the synthesised nano-{Fe-BTC} MOFs show similar bands, including in the 650–1800 cm^{-1} region, which is generally considered to be a fingerprint

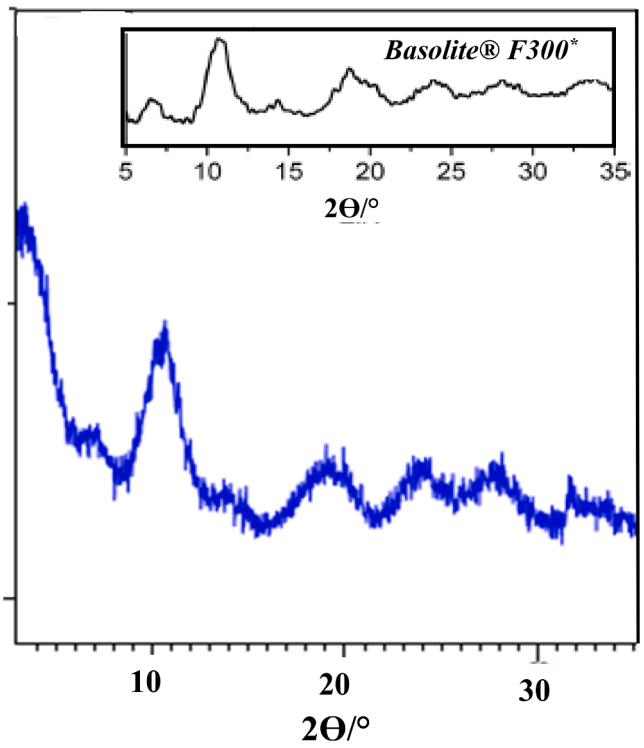

Fig. 2. PDRX of XRD patterns of the nano-{Fe-BTC} MOF synthesised (smoothed using Fourier filter in software HighScore de Panalytical) and Basolite®F300 (inset, *adapted from Peña-Méndez et al., 2020.

of MOFs. However, differences in intensity between the two materials are found in the 950–1300 cm^{-1} region (Fig. 3). The results of TGA analysis (Fig. 1S) corroborated a similar behaviour of synthesized and commercial Fe-BTC materials showing their thermal stability. This property, together with its stability in water, is required for the practical application of the synthesised material.

The adsorption capacity of MOFs is related to their surface areas. The porosity of nano-{Fe-BTC} MOF and commercial Basolite®F300 was determined by N_2 adsorption–desorption isotherms at 77 K (Table 2,

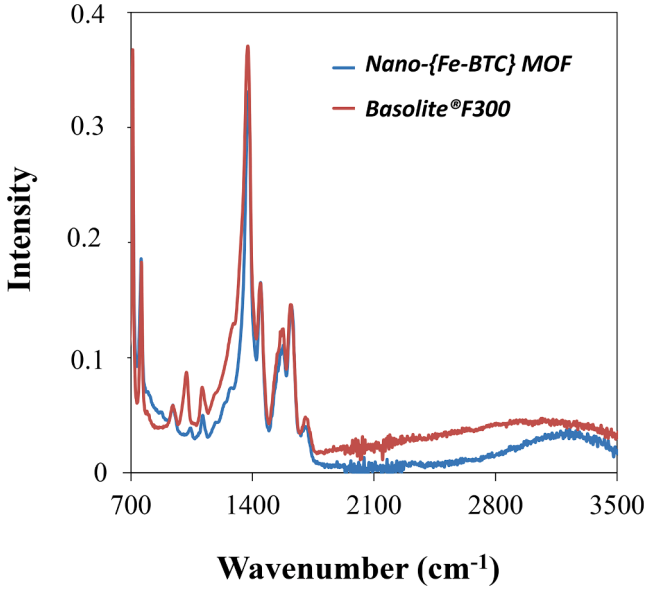

Fig. 3. Infrared spectra of the commercial Basolite® F300 and the nano-{Fe-BTC} MOF synthesised.

Table 2
Comparing adsorption efficiencies of different commercial MOFs, M-BTC (Basolite®F300, Basolite® C300) and Basolite® Z377. Experimental conditions: pH = 4, T = 298 K.

Sorbents	Adsorption Efficiency (%)		
	Br-FL	*FL*	*Cl-FL*
Basolite®F300	91.98	88.65	89.27
Basolite® C300	61.58	25.48	47.81
Basolite® Z377	3.48	1.43	0
Nano-{Fe-BTC} MOF*	*98.58*	*98.04*	*99.15*

*Synthesized in this work.

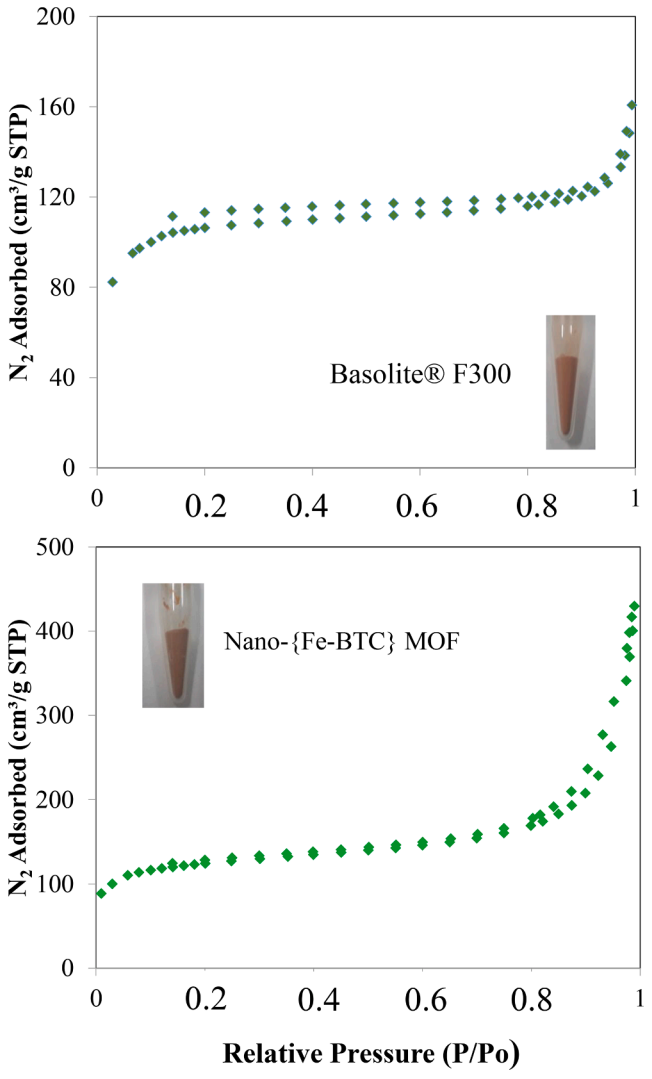

Fig. 4. Adsorption-desorption N_2 isotherms for Basolite®F300 and nano-{Fe-BTC} MOF.

Fig. 4). On comparing the results obtained, a larger amount of N_2 uptake was observed for the synthesized nanomaterial than for Basolite®F300, especially in the $P/P_0 < 0.2$ region. At the $0.2 < P/P_0 > 0.7$ range, the nano-{Fe-BTC} MOF reached a plateau after an upward slope that is attributed to the filling of mesopores. This slope is more accentuated for nano-{Fe-BTC} MOFs than for Basolite®F300. In the $0.8 < P/P_0 < 1$ region, there is a sharper amount of N_2 uptake for nano-{Fe-BTC} (Fig. 4). This behaviour corresponds to mesopores with a diameter in the upper size range (between 2 nm and 50 nm). As for the nano-{Fe-BTC} MOFs, the curves displayed an intermediate mode between the micropores and mesopores (Nvetha et al., 2019). The synthesized material has a larger volume of pores than Basolite®F300 (Table 2). This finding suggests that the change of the pore volume and surface will have certain effects on the adsorption behaviour of the new material. To understand this difference, the t-plot method (Nvetha et al., 2019; Lowell et al., 2020) was used to study the pore size distribution. Fig. 5 presents the amount of N_2 adsorbed as a function of the thickness at the standard temperature. The deviation from linearity (downwards tendency) is related to the presence of micropores; micropore volume in nano-{Fe-BTC} MOFs is 0.115 cm^3/g, the total micropore surface area is 251.75 m^2/g, while the total surface area (BET) is 427.22 m^2/g. These results show that mesopores ($50 > d > 2$ nm) and micropores ($d < 2$ nm) are present in synthesized nano-{Fe-BTC} MOFs, explaining their higher pore volume (0.53 $cm^3 \cdot g^{-1}$) in comparison with Basolite®F300 (0.41 $cm^3 \cdot g^{-1}$). Furthermore, the synthesized nano-{Fe-BTC} MOF is more homogeneous, with a nanoparticle size distribution of 337.2 ± 39.90 nm (Fig. 2S), than the Basolite®F300 nanoparticles that agglomerate in the bulk state as can be seen in the TEM images, whereas nano-{Fe-BTC} MOFs present good dispersion and uniform size (Fig. 6).

3.2. Evaluation of the adsorption properties of nano-{Fe-BTC} MOFs focusing on the analyte's structure and nano-{Fe-BTC} MOFs–analyte interactions

The capacity of this nano-{Fe-BTC} MOF material to remove fluorescent dyes from water has been evaluated through its adsorption properties. Adsorption experiments were performed in batches, after confirming the stability of the material in water. The concentrations of the dyes in the solution before and after adsorption were determined by high-performance chromatography with fluorescence detection (HPLC-FL). The results obtained show that the nano-{Fe-BTC} MOF material presents greater efficiency in adsorbing fluorescent dyes than commercial MOFs (Table 2). The effect of the initial pH on the adsorption capacity of the synthesised material was studied in the 2–9 pH range, initial dye concentration (C_0) 200 $\mu g \cdot L^{-1}$, and at room temperature. The highest percentage of dye adsorption for Br-FL was obtained at pH 2 (90 %) whereas for FL and Cl-FL was at pH 4 with adsorption efficiency percentages of 80% and 76.5%, respectively. At pH values >6 these percentages significantly decreased to less than 10% (Fig. 7A). The pH of zero point charge (pH_{pzc}) of the adsorbent is used to explain whether the adsorption mechanism is electrostatic or follows another mechanism and is also an important parameter to understand the effect of pH on the adsorption process (Nistor et al. 2020). The pHpzc was determined by measuring the pH of a Nano-{Fe-BTC} MOF suspension in water and was found to be 4.

This fact is explained by the deprotonation at pH values > 6 of the –COOH and –OH functional groups of the MOF surface that become negatively charged ($pH > pH_{PZC}$), as do the adsorbate molecules (Cl-FL pKa 4, 5.19; Br-FL pKa 2.9, 4.5; FL pKa 6.4). The presence of bromide and chloride substituents in the molecules affects both the conformation of the dye molecules and their acid-base properties. The FL molecule lacks the Br substituent (Br-FL) or Cl substituent (Cl-FL), and the Br-FL and Cl-FL molecules have structural rigidity. Thus, the interactions between the dyes and the nano-{Fe-BTC}, which are mainly electrostatic and π-π interactions, contributed to facilitate their adsorption at pH < 5. Hence, it was decided to conduct the adsorption experiments at pH 4.

Experimental data of dye adsorption isotherms was analyzed by applying the Langmuir and Freundlich isotherm models (Fig. 7B). Non-linear regression analysis was then applied to calculate the optimum adsorption parameters (Table 1S). The selection of the model that best fits the experimental data was made by the determination coefficient (R^2) and chi-squared (χ^2) values (Nistor et al. 2020). As can be seen in Table 1S, the highest R^2 and lowest χ^2 correspond to the Freundlich model with Br-FL having the highest K_F value (96.29), followed by Cl-FL (26.82) and FL (13.42). These differences in K_F are related to the affinity of the nanomaterials for the different anionic dyes, suggesting that the

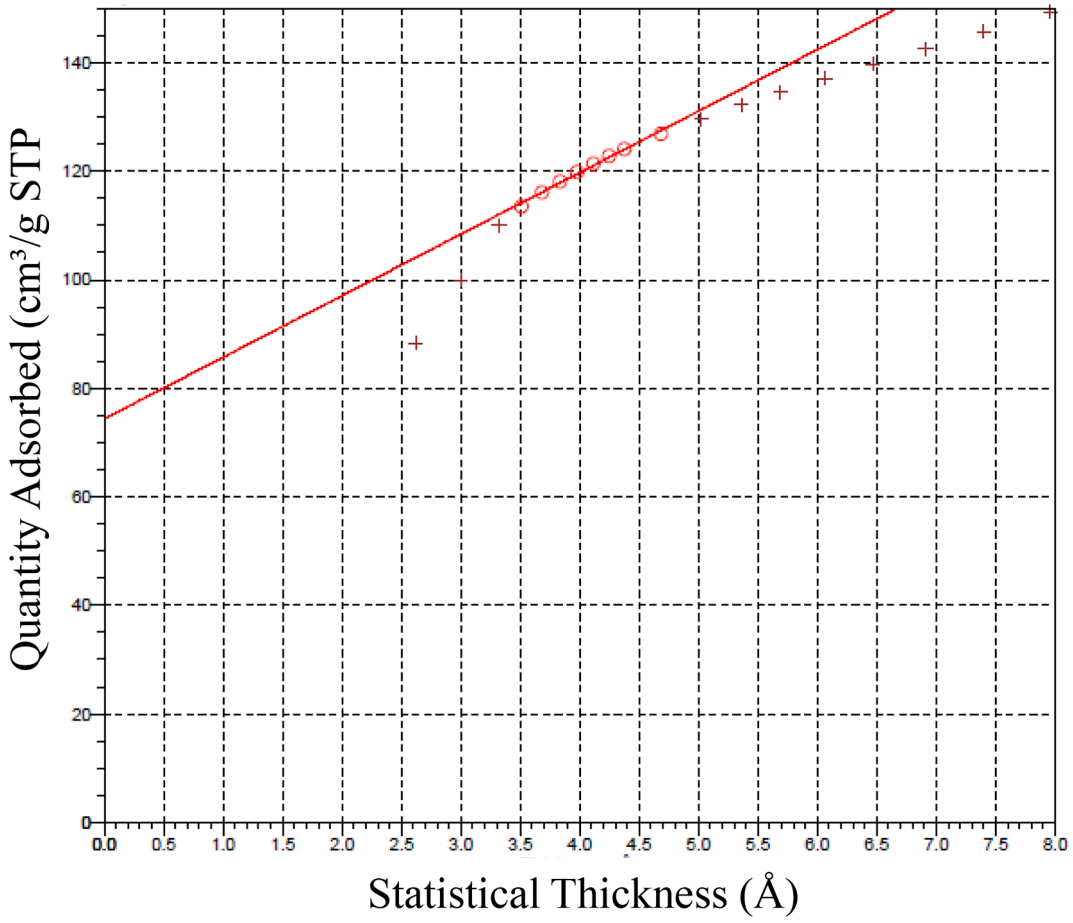

Fig. 5. t-Plot study.

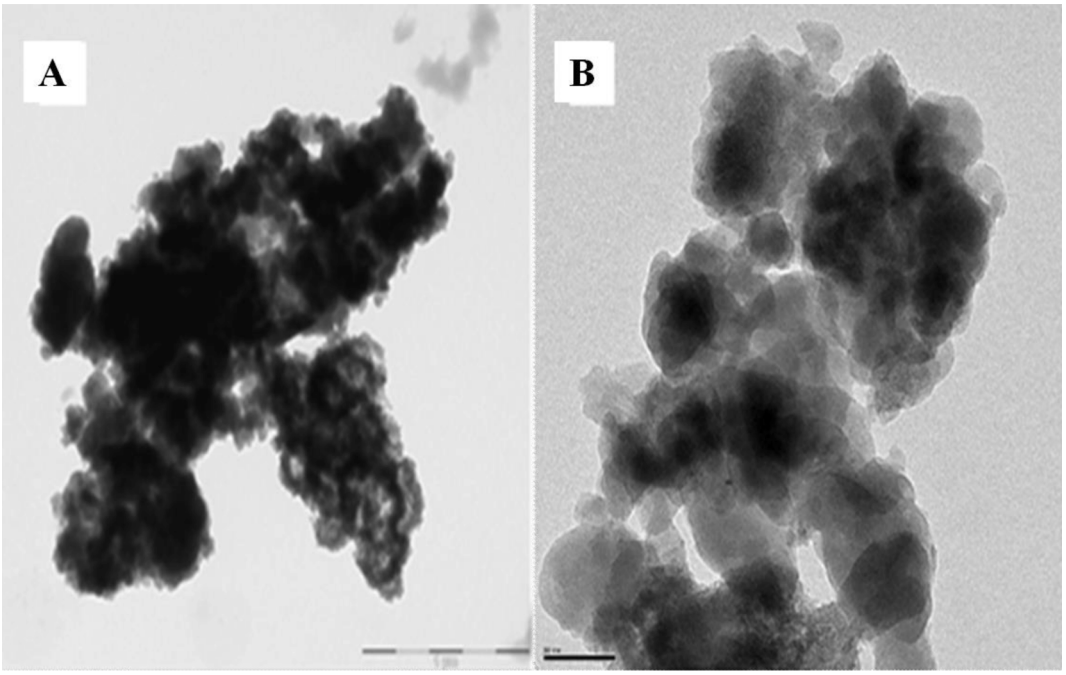

Fig. 6. TEM images of Basolite® F300 (A) and nano-{Fe-BTC} MOF (B).

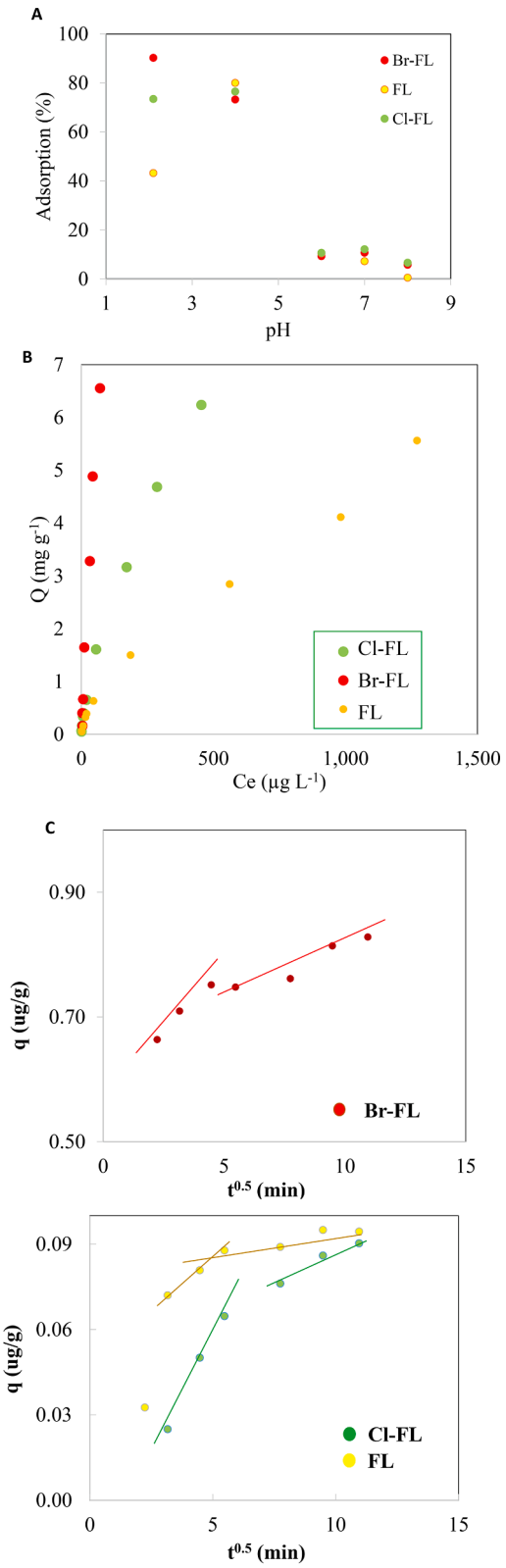

Fig. 7. (A) Effect of pH on the dyes adsorption efficiencies on nano-{Fe-BTC} MOF (B) Experimental data corresponding to Q (mg/g) vs Ce (µg L^{-1}) for FL, Cl-FL and Br-FL (C) Intra-particle diffusion studies for fluorescence dyes.

presence and the number of bromine and chlorine substituents in the fluorescent dyes affect their absorption behaviour. This fact can be ascribed to the importance of how their 3D molecule configuration interacts with the nanomaterial in comparison with that of FL (Zhao et al., 2019). The FL molecule lacks the Br substituent (Br-FL) or Cl substituent (Cl-FL), having Br-FL and Cl-FL molecules structural rigidity. All the dyes molecules have aromatic rings then π-π interactions may contribute to dyes adsorption playing a significant role in their adsorption performance (Qiu et al. 2017; Forgan, 2019; Zhao et al. 2019).

The results of the kinetic studies (Table 2S) correlate well with a pseudo-second-order model for all fluorescent dyes with pseudo-second-order velocity constants (k_2): Br-FL ($k_2 = 1.703$) > Cl-FL ($k_2 = 0.462$) > FL ($k_2 = 0.437$) indicating the importance of chemisorption (Table 2S). The equilibrium adsorption capacity calculated from the pseudo-second-order model, q_e (mg·g^{-1}), follows the order Br-FL (0.836 mg·g^{-1}) > FL (0.106 mg·g^{-1}) ~ Cl-FL (0.100 mg·g^{-1}). The presence of four Br atoms as substituents in the fluorescein molecule may explain the higher adsorption capacity of nano-{Fe-BTC} MOF for Br-FL in comparison with Cl-FL and FL, which have similar capacities although the molecule of Cl-FL has two chlorides as substituents atoms. The intra-particle diffusion model was employed in order to better understand the adsorption mechanisms of fluorescent dyes by the synthesised nano-{Fe-BTC} MOF. The results obtained show that the adsorption process consists of multiple steps, and that the surface of nanomaterial and intra-particle diffusions seem to play an important role in the rate-limiting step (Fig. 7C).

3.3. *The role of inorganic and organic complexing agents*

The effect of the presence of inorganic (chloride, nitrite, nitrate, phosphate and sulphate) anions in aqueous media at three different concentration levels, and organic matter (humic and fulvic acids) on the adsorption capacity of the nano-{Fe-BTC} MOFs was also evaluated (Fig. 3S). The effects of organic matter, represented by HA and FA, and different inorganic anions were not significant. However, in the case of phosphate, there was a decrease in the adsorption of FL and Cl-FL to 75% when its concentration was increased to 300 mg·L^{-1}. This may be due to the interaction of phosphate with the nano-{Fe-BTC} MOF. A possible Fe-phosphate interaction has been described in the literature (Xiaoshi et al., 2016; Peña-Méndez et al., 2020) and may also cause instability in the material.

3.3.1. *Application of D-SPE for the extraction of anionic dyes from water samples*

Once the fluorescent dyes were adsorbed by the nano-{Fe-BTC} MOFs, the possibility of recovery was evaluated as part of a recycling process, including the sorbent and the adsorbate, as is recommended in the best practices for green chemistry. The efficiency of the elution/recovery process of the fluorescent dyes depends on the magnitude of the host–guest interaction of the adsorption process versus the solvent-guest interactions. The adsorption capacity of the nano-{Fe-BTC} MOF material towards fluorescent dyes was investigated by spiking 10 mL of a water sample (tap water, mineral water, seawater and wastewater) with a mixture of dyes at a concentration level of 200 µg·L^{-1} each. Parameters such as the amount of sorbent and adsorption equilibrium time were studied, resulting in adsorption efficiencies of more than 90% for each of the dyes. After adsorption, different elution solvents and solvent volumes were evaluated in order to elute the fluorescent dyes adsorbed in the material (Fig. 8 A-C). The elution efficiencies were >90% when methanol containing 5% NH_3 was used for 5 min. The nano-{Fe-BTC} MOF material was then applied to the extraction of anionic dyes (200 µg·L^{-1} each) spiked to tap water, seawater and wastewater prior to their chromatographic determination. The results showed that the adsorption efficiency in percentage was only less than 65% in the case of wastewater. The low adsorption efficiency in this particular case may be due to the complexity of the matrix (Fig. 9) since The results obtained open

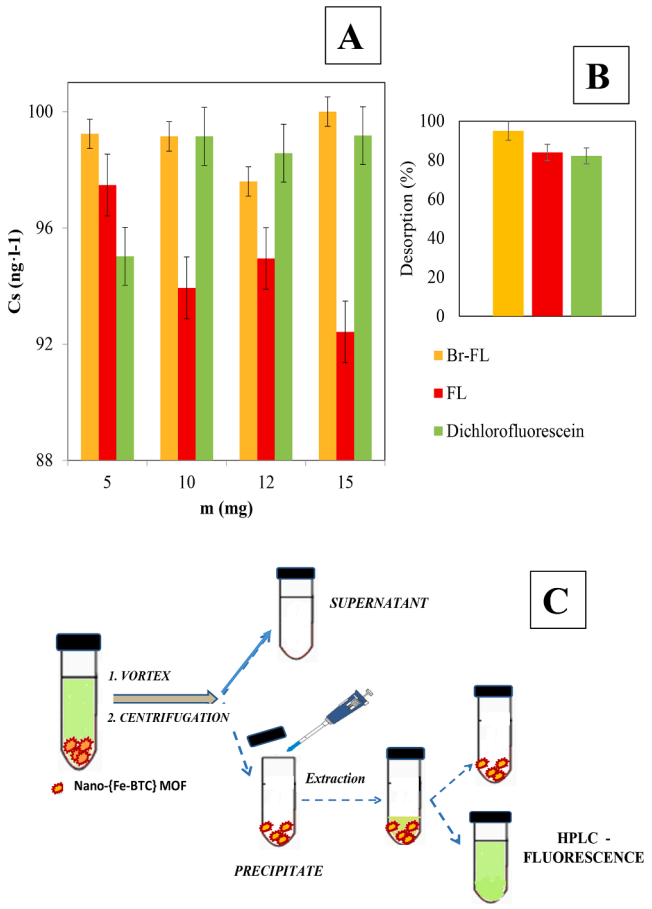

Fig. 8. (A-B) Results of the adsorption-desorption of dyes from aqueous solutions (pH 4, total volume for desorption 3 mL) (C) scheme of the optimized Dispersive Solid-Phase Extraction methodology.

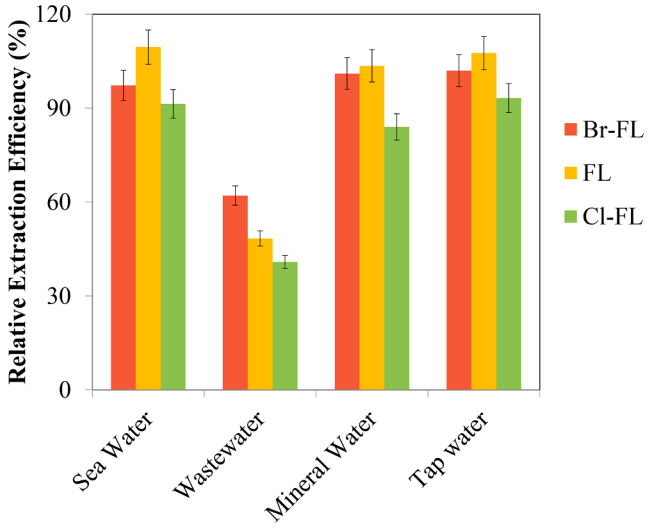

Fig. 9. Recovery expressed as adsorption efficiency (%) of dyes after release from developed nanomaterial nano-{Fe-BTC} MOF.

the possibility for the use of nano-{Fe-BTC} MOF materials both for water treatment and analytical applications. This is the first study not only to describe the adsorption of fluorescent dyes with these materials but also desorption in percentages of ~100%. These good results may be due to the specific loading capacity values as well as the release profiles, depending on the material design, synthesis, and framework chemistry.

4. Conclusions

A high porous nano-{Fe-BTC} MOF material was synthetized using a direct and green methodology (simple, short synthesis time in room conditions, no toxic organic solvents, low cost), which may provide improved conditions that give rise to further interesting applications. The adsorption capability of the synthesized material was tested for anionic fluorescent dyes, which were chosen as model organic compounds. The high values of equilibrium adsorption capacity for Br-FL (0.836 $mg{\cdot}g^{-1}$) > FL (0.106 $mg{\cdot}g^{-1}$) ~ Cl-FL (0.100 $mg{\cdot}g^{-1}$), enable the fast adsorption and detection of fluorescent dyes at trace and sub-trace levels in the water, and even in complex water matrices such as seawater. However, in the case of wastewater, the adsorption efficiency decreased due to a matrix effect. The elution of the adsorbed dyes from the sorbent is fast, using a small volume of methanol (5% NH_3), and does not result in degradation. To the best of our knowledge, there are no similar studies using nano-{Fe-BTC} MOFs to permit the efficient removal and recovery of fluorescent anionic dyes from water.

CRediT authorship contribution statement

José Elías Conde-González: Conceptualization, Formal analysis, Funding acquisition, Investigation, Methodology, Resources, Supervision, Writing - review & editing. **Eladia M. Peña-Méndez:** Conceptualization, Formal analysis, Funding acquisition, Investigation, Software, Supervision, Writing - review & editing. **Alba M. Melián-Fernández:** Investigation, Methodology. **Josef Havel:** Investigation, Resources, Writing - review & editing. **Victoria Salvadó:** Investigation, Resources, Writing - review & editing.

Declaration of Competing Interest

The authors declare that they have no known competing financial interests or personal relationships that could have appeared to influence the work reported in this paper.

Acknowledgements

E.M. P-M., J.E. C.-G. would like to thank the Ministry of Economy and Competitivity (Spain), project Ref. MAT2017-89207-R.

Appendix A. Supplementary data

Supplementary data to this article can be found online at https://doi.org/10.1016/j.enmm.2021.100541.

References

Aderonke, A., Idowu, O., Olugbenga, S., Bello, M., 2012. Metal organic frameworks as adsorbents for dye adsorption: overview, prospects and future challenges. Toxicol. Environm. Chem. 94, 1846–1863. https://doi.org/10.1080/02772248.2012.744023.

Alan, Y.L., Tang, C.K., 2014. Textile dyes and human health: a systematic and citation network analysis review. Color. Technol. 245–257 https://doi.org/10.1111/cote.12331.

Alvarez, A., Stanislav, M., Trashina, M., Cuykx, A., Covacib, K., De Waela, K., Janssens, D., 2017. Photodegradation mechanisms and kinetics of Eosin-Y in oxic and anoxic conditions. Dyes Pigm. 145, 376–384. https://doi.org/10.1016/j.dyepig.2017.06.031.

Amarajothi, D., Alvaro, M., Horcajada, P., Gibson, E., Vishnuvarthan, M., Vimont, A., Greneche, J.M., Serre, C., Daturi, M., Garcia, H., 2012. Comparison of porous iron Trimesates Basolite F300 and MIL-100(Fe) as heterogeneous catalysts for Lewis acid

and oxidation reactions: Roles of structural defects and stability. ACS Catal. 2, 2060–2065. https://doi.org/10.1021/cs300345b.
Bennett, T.D., Cheetham, A.K., 2014. Amorphous metal-organic frameworks. Acc. Chem. Res. 475 (2014), 1555–1562. https://doi.org/10.1021/ar5000314.
Bennett, T.D., Goodwin, A.L., Dove, M.T., Keen, D.A., Tucker, M., Barney, E.R., Soper, A. K., Bithell, E.G., Tan, J.C., Cheetham, A.K., 2010. Structure and properties of an amorphous metal–organic framework. Physical Rev. Lett., 104, 115503–115507. https://doi.org/10.1103/PhysRevLett.104.115503.
Castro-Alférez, M., Polo-López, M.I., Fernández-Ibáñez, P., 2016. Intracellular mechanisms of solar water disinfection. Sci. Rep. 6, 38145. https://doi.org/10.1038/srep38145.
Chatha, S.A.S., Asgher, M., Asgher, R., Hussain, A., Iqbal, Y., Hussain., S., Bilal., M., 2019. Environmentally responsive and anti-bugs textile finishes – recent trends, challenges, and future perspectives. Sci. Tot. Environ., 690, 667–682. https://doi.org/10.1016/j.scitotenv.2019.06.520.
Cheetham, A., Bennet, T., Coudert, F.-X., Goodwin, D., 2016. Defects and disorder in metal organic frameworks. Dalton Trans. 45 (2016), 4113–4126. https://doi.org/10.1039/C5DT04392A.
Commission notice on technical guidance on the classification of waste (2018/C 124/01), Official Journal of the European Union.
Diercks, S., Kalmutzki, N., Diercks, J., Yaghi, O.M., 2018. Conceptual advances from Werner complexes to metal−organic frameworks. ACS Cent. Sci. 4, 1457–1464. https://doi.org/10.1021/acscentsci.8b00677.
Commission Decision of 18 December 2014 amending Decision 2000/532/EC on the list of waste pursuant to Directive 2008/98/EC of the European Parliament and of the Council (Text with EEA relevance) (2014/955/EU). http://data.europa.eu/eli/dec/2014/955/oj.
EPA 820-R-11-003, 2011. Drinking Water Treatment Plant Residuals Management Technical Report. EPA. https://doi.org/10.1021/acscentsci.8b00677.
EPA530-F-05-004, 2005. Documents Related to the Hazardous Waste Listing of Dyes and Pigments. https://www.epa.gov/osw.
Forgan, R.S., 2019. The surface chemistry of metal–organic frameworks and their applications. Dalton Trans. 48, 9037–9042. https://doi.org/10.1039/C9DT01710K.
Horcajada, P., Chalati, T., Serre, C., Brigitte, G., Sebrie, C., Baati, T., Eubank, F., Heurtaux, D., Clayette, P., Kreuz, C., Chang, J.S., Hwang, Y., Marsaud, V., Bories, P. N., Cynober, L., Gil, S., Férey, G., Couvreur, P., Gref, R., 2010. Porous metal–organic-framework nanoscale carriers as a potential platform for drug delivery and imaging. Nat. Mater. 9 https://doi.org/10.1038/nmat2608.
Hossain, A., Sadique, A.B.M., Rayhan, R., Raihan, A., Nargis, M.I., Iqbal, A., Habib, A., Jafar, M., 2016. Kinetics of degradation of Eosin Y by one of the advanced oxidation processes (AOPs) -Fenton's process. AJAC 7, 863–879. https://doi.org/10.4236/ajac.2016.712074.
Lee, A., Yeoung, J., Chung, Y.G., Ri, H., Moon, R., 2019. Elucidation of flexible metal-organic frameworks: research progresses and recent developments. Coord. Chem. Rev. 389, 161–188. https://doi.org/10.1016/j.ccr.2019.03.008.
Lilly, J.L., Gottipati, A., Cahall, C.F., Agoub, M., Berron, B.J., 2018. Comparison of eosin and fluorescein conjugates for the photoinitiation of cellcompatible polymer coatings. PLoS ONE 8. https://doi.org/10.1371/journal.pone.0190880.
Lowell, S., Shields, J.E., Thomas, M.A., Thommes, M., 2019. Mesopore Analysis. In: Characterization of Porous Solids and Powders: Surface Area, Pore Size and Density. Kluwer Academy Publishes. Springer Nature Switzerland AG. Part of Springer Nature. 121-128. ISBN 978-1-4020-2303-3.
McAvoy, S.A., 2014. Global Regulations of Food Colours. Each Region has its own definitionsof what constitutes a color additive, with related use requirements and restrictions. The Manufacturing Confectioner, September, 77–86.
Mohamed, A., El Nemr, H.A., 2017. Health and environmental impacts of dyes: mini review. Environ. Sustain. 1, 64–67. https://doi.org/10.11648/j.ajese.20170103.11.
Nistor, M.A., Muntean, S.G., Maranescu, B., Visa, A., 2020. Phosphonate metal–organic frameworks used as dye removal materials from wastewaters. Appl. Organomet. Chem. 34, 5939. https://doi.org/10.1002/aoc.5939.
Nvetha, R., Kollu, P., Chandar, K., Pitchaimuthu, S., Jeong, S.K., Grace, A.N., 2019. Role of MIL-53(Fe)/hydrated–dehydrated MOF catalyst for electrochemical hydrogen evolution reaction (HER) in alkaline medium and photocatalysis. RSC Adv. 9, 3215–3223. https://doi.org/10.1039/C8RA08208A.
Oliveira, E., Bartolo, E., NfflÇez, C., Pilla, V., Santos, H., Fernández-Lodeiro, J., Fernández-Lodeiro, A., Djafari, J., Capelo, J.L., Lodeiro, C., 2018. Green and red fluorescent dyes for translational applications in imaging and sensing analytes: a dual-colour flag. Chem. Open 7, 9–52. https://doi.org/10.1002/open.201700177.
Ortiz-Perea, N., Gander, R., Abbey, O., Callaghan, A., 2018. The effect of pond dyes on viposition and survival in wild UK *Culex* mosquitoes. PLoS ONE 2, 1–15. https://doi.org/10.1371/journal.pone.0193847.
Peña-Méndez, E.M., Mawale, R.M., Conde-González, J.E., Socas-Rodríguez, B., Havel, J., Ruiz-Pérez, C., 2020. Metal organic framework composite, nano-Fe3O4@Fe-(benzene-1,3,5-tricarboxylic acid), for solid phase extraction of blood lipid regulators from water. Talanta, 207.https://doi.org/10.1016/j.talanta.2019.120275.
Pereira, L., Alves, M., 2012. Dyes-Environmental Impact and Remediation. In, Environmental Protection Strategies for Sustainable Development. Editors A. Malik, E. Grohmann. Springer, Dordrecht. ISBN 978-94-007-1591-2. https://doi.org/10.1007/978-94-007-1591-2_4.
Pilloni, M., Padella, F., Ennas, G., Lai, S., Bellusci, M., Rombi, E., Sini, F., Pentimalli, M., Delitala, C., Scano, A., Cabras, V., Ferino, I., 2015. Liquid-assisted mechano chemical synthesis of an iron carboxylate Metal Organic Framework and its evaluation in diesel fuel desulfurisation. Microporous Mesoporous Mater. 213, 14–21. https://doi.org/10.1016/j.micromeso.2015.04.005.
Ponnusamy, S., Saravanan A., 2017. Sustainable wastewater treatments in textile sector. The Textile Institute Book Series, 323-346. https://doi.org/10.1016/B978-0-08-102041-8.00011-1.
Preiß, T., Zimpel, A., Wuttke, S., Rädler, J., 2017. Kinetic analysis of the uptake and release of fluorescein by metal-organic framework nanoparticles materials. Materials 10, 214–216. https://doi.org/10.3390/ma10020216.
Qiu, J., Xiong, Y., Zhang, F., Jian, M., Yao, F., 2017. Acid-promoted synthesis of UiO-66 for highly selective adsorption of anionic dyes: Adsorption performance and mechanisms. J. Colloid & Interfaces Sci., 499, 151–158. https://doi.org/10.1016/j.jcis.2017.03.101.
Sánchez-Sánchez, M., de Asua, I., Ruano, D., Diaz, K., 2015. Direct synthesis, structural features, and enhanced catalytic activity of the Basolite F300-like semi-amorphous Fe-BTC framework, 44498–4506l Cryst. Growth Des. 15. https://doi.org/10.1021/acs.cgd.5b00755.
Tao, S., Jiancan, C.Y., Yu, Y., Guodong, Q., 2016. Encapsulation of dyes in metal–organic frameworks and their tunable nonlinear optical properties. Dalton Trans. 45, 4218–4223. https://doi.org/10.1039/C5DT03466C.
UNESCO 2015, 2015. Unsustainable world. In The UN World Water Development Report 2015, Water for a Sustainable World. United Nations Educational, Scientific and Cultural Organization, Paris, France, 10-12. ISBN 978-92-3-100071-3.
Xiaokun, C., Bo, W., 2016. Water purification: adsorption over metal-organic frameworks. Chin. J. Chem. 34, 175–185. https://doi.org/10.1002/cjoc.201500761.
Xiaoshi, H., Xiaobing, L., Chao, L., Yanqun, N., Yuxing, L., Qun, C., Eugéne, M., Ming, S., Bingwen, H., 2016. Facile synthesis of the Basolite F300-like nanoscale Fe-BTC framework and its lithium storage properties. RSC Adv. 6 (2016), 114483–114490. https://doi.org/10.1039/C6RA22738D.
Zhao, X., Zhao, Y., Zheng, M., Liu, S., Xue, W., Du, G., Wang, T., Gao, X., Wang, K., Hu, J., Gao, Z., Huang, H., 2019. Efficient separation of vitamins mixture in aqueous solution using a stable zirconium-based metal-organic framework. J. Colloid & Interface Sci. 555, 714–721. https://doi.org/10.1016/j.jcis.2019.08.024.